SPATIAL AND LAYER-CONTROLLED VARIABILITY IN FRACTURE NETWORKS

Andrew Procter[1] and David J Sanderson[1,2]

[1] Ocean and Earth Science, University of Southampton, National Oceanography Centre, Southampton SO14 3ZH, UK

[2] Faculty of Engineering and Environment, University of Southampton, Southampton SO17 1BJ, UK.

*Corresponding Author: Professor David J Sanderson,

Address: Building 7, Room 5030, Faculty of Engineering and the Environment, University of Southampton, Southampton SO17 1BJ.

Email: d.j.sanderson@soton.ac.uk

Abstract

Topological sampling, based on 1) node counting and 2) circular sampling areas, is used to measure fracture intensity in surface exposures of a layered limestone/shale sequence in north Somerset, UK. This method provides similar levels of precision as more traditional line samples, but is about 10 times quicker and allows characterization of the network topology. Georeferencing of photographs of the sample sites allows later analysis of trace lengths and orientations, and identification of joint set development.

ANOVA tests support a complex interaction of within-layer, between-layer and between-location variability in fracture intensity, with the different layers showing

anomalous intensity at different locations. This variation is not simply due to bed thickness, nor can it be related to any obvious compositional or textural variation between the limestone beds. These results are used to assess approaches to the spatial mapping of fracture intensity.

Key words: Fracture, network, topology

1. Introduction

The presence of a fracture network within a rock mass may significantly influence bulk rock properties such as porosity, permeability and rock strength (e.g. Long and Witherspoon, 1985; Palmstrøm, 1996; Larsen and Gudmundsson, 2010). Understanding the controls on bulk rock properties and the spatial distribution of fractures is vital for the engineering and petroleum industries (e.g. Quesada et al., 2009; Macias et al., 2014). Many factors are important in understanding fracture systems and predicting physical processes such as fluid flow and deformation, for example size-frequency scaling (e.g. Odling, 1997; Marrett et al., 1999; Ortega et al., 2006) and the fracture type, aperture, connectivity and mineral fill (e.g. Olson et al., 2009) that may modify the transmissibility of the fracture system (e.g. Antonellini and Aydin, 1994; Zimmerman and Main 2003).

In this paper we focus on two necessary prerequisites to analysing and modelling the spatial variability of fracture networks in surface exposures:

1) The development of methods that are efficient enough to allow adequate sampling of the network.

2) Understanding the main sources of variability in such networks, so that these may be incorporated into the experimental design of any fracture survey.

Fracture network characterisation commonly uses measurement of data, either along scanlines (e.g. Priest and Hudson, 1981) or by trace mapping (e.g. Odling, 1997).

Fracture length, orientation and spacing are commonly measured and data collection can be a time consuming process (Villaescusa and Brown, 1992; Wu and Pollard, 1995). An alternative way to analyse a fracture network will be described that uses a topological approach to data collection and interpretation (Sanderson and Nixon, 2015) and mainly involves counting rather than measuring of fractures.

In most sedimentary sequences, fractures are strongly layer-controlled (e.g. Helgeson and Aydin, 1981; Afşar et al., 2014), with different rock units and thicknesses influencing the intensity and nature of the fracture networks. Thus, to understand the spatial variability of the fractures requires an assessment of the within-layer and between-layer variability. We describe a series of experiments designed to allow statistical assessment of this variability through a series of ANOVA (analysis of variance) tests. The characteristics analysed in this study are mainly fracture intensity and connectivity. Intensity is defined as the total measured fracture length per unit area (e.g. Singhal and Gupta, 2010). Fracture intensity gives a direct indication of fracture abundance within a rock mass (Ortega et al., 2006), where fractures are measured as either number of fractures per length (P_{10}) or total fracture length per area (P_{21}).

2. Methodology

2.1 Region of investigation

The study area is located on the southern margin of the Bristol Channel Basin, on the north coast of Somerset, between Kilve and East Quantoxhead (Fig. 1). The E-W trending Mesozoic basin developed during N-S extension, which may have initiated in the Triassic, but the main extension faulting occurred in the early Cretaceous ((Chadwick, 1986; Van Hoorn, 1987; Peacock and Sanderson, 1999). The basin was inverted during the Eocene and Oligocene as N-S compression produced reactivation of the normal faults and development of conjugate sets of cross-cutting strike-slip

faults (Dart et al., 1995; Peacock and Sanderson, 1999). The open fractures (or joints) are generally later than the faults and formed during subsequent uplift to their present-day exposure at the surface (Rawnsley et al., 1998; Engelder and Peacock, 2001). The fact that faults and associated veins are extensively infilled by calcite but the joints are not, supports the more recent age of the latter.

Data were collected from coastal exposures of an interbedded sequence of shale-marl-limestone from the lower Jurassic (Hettangian – Sinemurian), known locally as the Blue Lias Formation (Whittaker and Green, 1983; Sheppard et al., 2006). The area was chosen because of the excellence of the exposure on a wave-cut platform and the marked difference in the intensity and form of joints in the limestones and shales and marls, hereafter referred to simply as shales.

Since a primary aim of the study was to investigate the role of layering, the same five limestone beds were targeted for analysis (Fig. 2) as they can be easily identified at several locations along the coast. The limestone beds were assigned a number (as Fig. 2); based on the stratigraphy established by Whittaker and Green (1983), and we use the term 'bed', rather than layer, where specifically referring to one or more of these units. The limestone beds range from 20 to 50 cm in thickness and are separated by shales and marls, typically 1 m or so thick. Beds 155 and 157 are 40-50 cm thick, whereas beds 159 and 161 are 15-25 cm thick; the five beds cover the range of thicknesses of the more prominent limestones in the Blue Lias, although some thinner beds occur. Focussing the data interpretation on the same five beds allows for more reliable and robust analysis of the fracturing and comparison of its development at different locations (experiments).

Four experimental areas were set up in order to statistically analyse the within-layer and between-layer variation using analysis of variance (ANOVA) techniques (Fig. 3). In Experiments 1 and 2, we were able to obtain multiple samples from beds 155, 157, 159, 161 and 165. At 3 and 4, we were not able to sample beds 155 and 165. A total

of 65 samples are used in these four experiments, 56 from the targeted limestone beds, 3 from additional thin limestones and 6 from the Kilve Shales that overlie the Blue Lias.

All the fractures studied are open joints that form at a high angle (generally >75°) to layering. We use the term 'joint' when referring specifically to these studied structures and 'fractures' when referring more generally. The joints are generally layer-bound (Fig. 2), i.e. they terminate at the top and bottom of the limestone beds, only rarely passing into the adjacent marls and shales, i.e. bed-bound (Hooker et al., 2013). The joints form a network of well-connected fractures that are exposed on the bedding surfaces.

2.2 Topological sampling

A topological study involves examining the dimensionless properties of the fault network, characterising the spatial relationships between the fractures. The topological approach to fracture characterisation is discussed in detail by Sanderson and Nixon (2015) and will be applied throughout this paper. The topology of a fracture network can be described by a system of branches (or segnents) and nodes, where a branch is part of a fracture trace with a node at each end (Fig. 4). Nodes can be assigned to one of three categories, I-nodes (isolated tips), X-nodes (cross-cutting fractures) and Y-nodes (one fracture abutting another) and the proportion of these can be used to define network characteristics (Sanderson and Nixon, 2015); for example, the proportions of I-, Y- and X-nodes can be represented on a triangular plot (Fig. 4c). The proportion of nodes is invariant to continuous distortions, whereas the geometry of the fractures is not, hence it is a topological feature of the network. Topology is commonly utilised to determine spatial relationships between fracture sets, such as connectivity.

Sanderson and Nixon (2015) demonstrate that nodes and branches may also be used to help estimate geometric properties of fracture networks. For example, counting the number and type of nodes within a known area provides basic estimates of node and branch frequency – where frequency is a number per unit area, with dimensions $[L]^{-2}$. The node frequency (N_N) is simply:

$$N_N = (N_I + N_Y + N_X) \quad (1)$$

Each I-node represents the end of one branch, a Y-node the end of three branches and a X-node the end of four branches. Since each branch has two ends, the number of branches (N_B) is given by:

$$N_B = (N_I + 3N_Y + 4N_X) / 2 \quad (2)$$

Since a Y-node generally represents the abutting tip of a fracture and an I-node the isolated tip, whereas an X-node represents no tips, it follows that the number of traces (N_L) is given by:

$$N_L = (N_I + N_Y) / 2 \quad (3)$$

If the total length of fracture traces (ΣL) or intensity ($I = \Sigma L/\text{area}$) is known, it is easy to calculate the average trace length $\langle L \rangle = \Sigma L / N_L$ or branch length $\langle B \rangle = \Sigma L / N_B$.

2.3 Field procedure

The methodology used to collect and interpret data in this study is summarised in Fig. 5. Fracture data were collected using circular scanlines (Mauldon et al., 2001; Rohrbaugh et al., 2002) and node counting (Sanderson and Nixon, 2015). Sample sites were selected based on the extent and quality of the exposed bedding surfaces, with each sample being approximately equally spaced along the available exposure at each experiment.

The field procedures produce a rapid estimate of fracture intensity (P_{10}), based on counting the edge-nodes (N_E), i.e. the traces that intersect the circumference of the

circle. A circle is used since it is a line that equally represents all directions within the surface and Mauldon et al. (2001) demonstrate that a weighting of π/2 can be used to correct the number lines intersecting the circle. Thus the N_E counts (Fig. 4b) provide a 1-D estimate of fracture intensity, P_{10}, given by:

$$P_{10} = (N_E / \text{circumference}) \cdot \pi/2 \qquad [L^{-1}] \qquad (4)$$

At each individual site, a circle was drawn with chalk onto the surface of the bed, together with a cross oriented N-S and E-W (Fig. 6a). The initial aim was to draw a 1 m radius circle at all sites, however, where bedding surfaces were too narrow to permit this, four adjacent 0.5 m radius circles were used. By halving the radius of the circle from 1 m to 0.5 m, the perimeter decreases by a factor of ½ and area by a factor of ¼. Therefore, four 0.5 m radius circles produce the same area at each site. For further analysis, the counts of nodes within the circle were simply summed for the four areas, with the total number of edge nodes being halved to get the equivalent for a 1 m circle.

To facilitate the counting of nodes, small plastic disks (counters) were placed at each node (Fig. 6a), with different colours used to identify the node types. Edge-nodes (E) were located at the intersections of fractures with the circle and I-, Y- and X-nodes located within the circle. The disks allowed a visual check that all nodes had been identified and, when node identification was complete, a photograph was taken to record the site. A count of each type of node was made as the disks were removed (N_E, N_I, N_X and N_Y). The bed number, its thickness and the circle radius were also recorded for each sample. The edge nodes are then used to estimate the intensity (P_{10}) using equation (4). Photographs of the fractures within the circle were later used for analysis of the branch lengths and hence a 2-D estimate of fracture intensity (P_{21}) – see below.

2.4 GIS analysis

A graphics package (Corel Photo-Paint) was used to remove the perspective distortion of the field photos (Fig. 6b), thus restoring the form of the sampling circular. The restored photos were then loaded into ArcGIS and the fracture network digitized and analysed. Alternatively, the field photographs can be rectified in a GIS, with subsequent digital analysis and interpretation processes shown in Fig. 5. Node types were digitized and classified as I-, Y- or X-nodes (Sanderson and Nixon, 2015). Branches were mapped as polylines, between each connected node and classified as either I-I branches, I-C branches or C-C branches, where C represents a tip at a connected node (i.e. Y or X). Branches with one node that was unidentified, or situated outside the sample circle, were designated as U-branches and include an E-node (Fig. 6c). The proportion of I, Y and X nodes were used to characterize the topology.

The mapped branches were scaled and georeferenced and the total branch length (ΣL) measured within the sample area (A) in the GIS. This was then used to estimate the 2-D fracture intensity, P_{21} (Dershowitz and Herda, 1992), which was calculated as follows:

$$P_{21} = \Sigma L / A \qquad [L^{-1}] \qquad (5)$$

P_{21} was plotted against P_{10} for Experiment 2, in order to determine whether P_{10} estimations could be used to directly calculate fracture intensity using purely node counts. Georeferenced coordinate data extracted from branch polylines in ArcGIS also allow calculation of branch orientation and were used to create rose diagrams representing the fracture network within each bed.

2.5 Statistical analysis

In this paper we mainly discuss data for the fracture intensity (P_{10}) as this provides a direct indication to the degree of fracturing that a rock mass has undergone (Singhal and Gupta, 2010). Intensity determined from the circular scanline is a 1-dimensional estimate and is designated P_{10}. Its variability within and between-layers was analysed statistically through one-way and two-way ANOVA, which was conducted using spreadsheets and the programme GraphPad Prism. Assuming reasonably homogeneous variances for each sample, a statistically significant result indicates that the mean fracture intensity varies between the beds. A *post-hoc*, multiple comparison test was completed, by way of t-test for one-way ANOVA and Sidak's test for two-way ANOVA, in order to identify significant differences between individual beds.

3. Results

3.1 Fracture intensity

The fracture intensities, obtained by edge-node counting on circular scanlines (P_{10}), range from 2 – 7.5 m^{-1}, with a mean of ~4.5 m^{-1}, equivalent to a mean spacing (1/ P_{10}) of ~0.22 m (Table 1). These values are similar to those obtained in other studies of these exposures (e.g. Afşar et al., 2014; Engelder and Peacock, 2001).

To evaluate the method based on counting, we plot the results for P_{10} against those for P_{21} in Experiment 2 (Fig. 7). This shows a strong linear correlation (R^2 = 0.93) with a slope of 1 and intercept ~0, indicating that the rapid evaluation of P_{10} gives an accurate and unbiased estimate of the fracture intensity (P_{21}). This is an important result as it validates the counting procedure used. We estimate that counting to determine P_{10} is ~10 times quicker than the length measurement required for P_{21} and provides a similar level of precision.

3.2 Within-layer and between-layer variability

Experiments 1 to 4 were designed to compare the variation in fracture parameters between and within limestone layers, using one-way ANOVA. The beds used in the experiments are given in Table 1. The initial plan was to collect three samples in each of five limestone beds (155, 157, 159, 161, 165) in three regions, which was met for Experiments 1 and 2. Experiment 1 conforms closely to the original design with 3x5 = 15 samples. Most of the beds were sampled using a 1 m radius circle, but we needed to use 0.5 m radius circles in Bed 159. In Experiment 2 we sampled some additional sites, particularly in Beds 155, 157 and 159. The third experiment was re-designed, since suitable surfaces of beds 155 and 165 were not available. Instead we changed the aims of Experiments 3 and 4 to compare the three available horizons within the footwall and hanging wall, respectively, of a large fault. Table 1 indicates the number of samples obtained and the average fracture intensity in each layer and the ANOVA for fracture intensity (P_{10}) from all four experiments is given in Table 2.

In Experiment 1, the between-layer, mean squared deviation (MSD) is only slightly greater that the pooled estimate of within-layer MSD, producing an F-ratio of 2.17. This is not significant at the 0.05 level (Table 2), indicating that there is no significant variation of fracture intensity between layers. Experiment 2, however, showed a significant between-layer variation at <0.01% level. Although only three layers were analysed in Experiments 3 and 4, one of these (4) showed a significant difference between layers whereas the other (3) did not. Box-and-whisker plots of the range (whiskers) and 95% confidence limits (boxes) illustrate the heterogeneity within the different experiments (Fig. 8).

These results indicate that there is some layer control on the fracture intensity, the significance of which varies from location to location. One-way ANOVA of bed thickness showed significant variation between layers at all sites. Various other

parameters were also tested, with average branch length <B> and dimensionless branch intensity (B_{11} = P_{10} <B>) both showing no significant variation between layers.

3.3 Two-way ANOVA

The data collected in Experiments 1-4 are characterised by two factors – (1) the bed number of the limestone layer and (2) the experiment number, which related to one of four different locations. The two-way ANOVA tests (Table 3) show that there is significant variation between both beds and experiments, generally at the <5% level, as well as variable interaction between these two factors. Comparison of Experiment 1 and 2 shows somewhat greater between-layer variation than between experiments (Table 3a). Overall, Experiment 1 has the higher intensities, with this mainly being due to higher intensities in Beds 159 and 165 (Fig. 8). Comparison of Experiments 3 and 4 shows somewhat greater between-experiment variation, with marginally significant between layer variation and no significant interaction (Table 3b). This is supported by the significantly higher intensities in Experiment 3, mainly due to the highly significant difference in Bed 157 (Fig. 8).

Taken together, the two-way ANOVA (Table 3) and box-and-whisker plots (Fig. 8) support a complex interaction of beds and location, with the different beds showing anomalous intensity at different locations. Thus any spatial mapping of the joint data would be expected to show both regional and layer-controlled variability, which we will discuss in more detail later.

3.4 Fracture intensity and bed thickness

Given that the joints are layer-bound and that fracture intensity sometimes, and bed thickness always, varies with beds in the experiments, we test the hypothesis that bed thickness could control fracture intensity. It should be remembered that the main experiments were restricted to limestones in the typical thickness range of the Blue Lias, i.e. 0.2 to 0.5 m and not designed to cover the full range of bed thicknesses. The

275 measured beds included two thinner (~0.2 m) layers (159, 161) and two thicker (~0.4 m)
276 layers (155, 157), with Bed 165 having an intermediate thickness (0.2 - 0.3 m). In addition,
277 we measured three samples in a very thin limestone (~0.1 m) in the Kilve Shales, above Bed
278 165, near experiment 1.

279 Figure 9a is a plot of P_{10} against layer thickness for all samples; similar plots for
280 individual experiments were also made. The plot shows that that there is no
281 correlation between bed thickness and fracture intensity (R^2 = - 0.0015). Figure 9b
282 summarizes the range and 95% confidence limits of the different groups of limestones,
283 indicating that there is no significant difference in fracture intensity between thicker
284 beds 155/157 ($<P_{10}> = 4.5 \pm 0.5\ m^{-1}$) and thinner beds 159/161 ($<P_{10}> = 4.7 \pm 0.5\ m^{-1}$), but the
285 three 'thin' limestones have a significantly higher intensity ($<P_{10}> = 6.0 \pm 0.3\ m^{-1}$). It is also
286 apparent from Fig. 8 that the layers with higher intensity include both the thinner layers
287 (159/161) and thicker layers (155/157), with no consistent variation between beds.

288 These data strongly suggest that bed thickness is not a primary control on fracture
289 intensity variation between layers. It must be emphasised that this result only applies
290 to a small interval of the Blue Lias, with a limited thickness range 0.2 – 0.5 m, and we
291 do not assume it applies more widely, even within the geological setting studied. The
292 important point is that we have established the existence of significant between-layer
293 variation that we cannot relate to bed thickness. Hence we go on to discuss other
294 possible factors.

295 ### *3.5 Limestone vs Shale*

296 In addition to the limestones, the shales within the Kilve Shales were also sampled at 6
297 sites and results included in Fig. 9b. The fracture intensity is much lower in the shales
298 ($<P_{10}> = 0.5 \pm 0.13\ m^{-1}$), and required larger sampling circles of radius 3 m. The fracture
299 intensity does not vary much within the shale, regardless of the bed thickness (range
300 from 0.35 m to 2 m).

3.6 Topology and joint sets

In this paper we primarily focus on the use of node counting to facilitate collection of intensity data from the joint networks, but we can also characterize the topology itself, although this is only discussed briefly here. In the limestones, the joints form highly connected networks dominated by Y-nodes (Fig. 10) and C-C branches. In the shales there are approximately equal proportions of I and Y nodes, and the networks are significantly less well-connected.

One important use of topology is to help establish the relative sequence of fractures. Relative age is generally determined by cross-cutting relationships, but the absence of observable displacements at the X-nodes of joints (opening mode fractures) precludes such analysis. Thus, I- and X-nodes are of little use, but the Y-nodes indicate abutting relationships (Hancock, 1985; Sanderson, 2015; Sanderson and Nixon, 2015), with a later joint stopping (abutting) against an earlier one. The abundance of Y-nodes in the joints allows us to recognise any systematic age relationships.

Based on the orientation and abutting relationships, we recognise five sets of joints in Experiment 2, as summarized in Table 4 (see also Sanderson 2015). Generally, only three sets are developed at any one sample site, and Set 2 is restricted to Bed 159 (Fig. 11). For example, in Fig. 6d we recognise 3 sets of joints: Set 1 - long, NW-SE trending joints (red-thick); Set 3 - E-W striking joints (green-thin) that generally abut Set 1 forming the Y-nodes; and Set 4/5 – short, curved joints generally N-NE striking (yellow-dashed) that generally abut Sets 1 and 2 forming Y-nodes.

The abutting relationships indicate a fairly consistent order of development of the joint sets (Fig. 11e), with 86% of the recorded Y-nodes confirming the order 1 → 5. The remaining 14% are attributed to 'back-cycling' due to the development of cross-joints between more closely spaced, earlier joints (c.f. Bai et al. 2002).

4. Discussion

4.1 Sampling procedure

In this study, we tested a new method of collecting fracture data on bedding surfaces. The method is based on the circular scanline approach of Mauldon et al. (2001) combined with the topological approach of Sanderson and Nixon (2015).

The fracture network is considered as a system of branches and nodes, and is characterized simply by counting different node types, which takes just a few minutes for each sample site. Direct measurement of branch lengths is possible in the field, but is very time-consuming, typically taking about 30 minutes per sample, and was not carried out routinely. The results (Fig. 7) show that P_{10} estimates compare well with the more traditional measurement of trace lengths (P_{21}). Watkins et al. (2015) consider this approach to be four times quicker than direct measurement of trace length; our experience suggests that it can be over 10 times quicker.

Photographs of the networks on bedding surfaces were rectified and digitizied in the GIS, mainly for subsequent topological analysis. Modern digital photo resolution allows measurement of trace lengths to ~1 mm precision and, with careful rectification, provides accurate estimates of 2-D intensity (P_{21}). This process takes almost as long as the field measurement of branch lengths and cannot be easily completed in the field.

Orientation, length and censoring bias are all problems encountered when using scanlines to collect data (Einstein and Baecher, 1983; Mauldon et al., 2001; Watkins et al., 2015). The circular scanline simplifies correction for directional bias (Mauldon et al., 2001; Rohrbaugh et al., 2002), provided fractures are all normal to the plane of the circle, as is often the case on bedding for many layer-bound fracture systems in sedimentary rocks. Thus the method removes the need for individual corrections for fractures based on the angle they make with the scanline – the Terzaghi correction

(Terzaghi, 1965; Priest and Hudson, 1981; Priest, 1993). Rohrbaugh et al. (2002) suggest that the circles need to be big enough to encounter ~30 fracture traces. Our 1 m radius circles intersected an average of ~20 fractures, but this was sufficient to provide a good correlation with direct measurement of fracture intensity by measurement of trace length within the circle.

In addition to the edge-nodes, we also counted the number of nodes within the circle, the 1 m radius circles having an average number of 36.5. These nodes provide important information:

(1) The proportions of different node types allow characterization of the topology using the approach of Manzocchi (2002) and Sanderson and Nixon (2015), as in Fig. 10. In our examples, this approach confirmed that the limestone-hosteed networks were well-connected and Y-node dominated fracture systems.

(2) The node counts also provide unbiased estimates of the number of traces and branches within the circle. The line frequency is essentially the same as the tip counting procedure used by Rohrbaugh et al. (2002), although we prefer to use the branch frequency for reasons discussed in Sanderson and Nixon (2015).

(3) Combining (2) with the estimate of intensity (P_{10}), allows estimation of average trace lengths and branch lengths. The average branch length <B> = 0.28 m is much less that the diameter of the circle, whereas the trace lengths have <L> = 0.83 m and many exceed the diameter of the circle.

4.2 Dominant controls on fracture network variability

It is widely recognised that fracture network characteristics are controlled by many processes (e.g. Nelson, 2001; Olson et al., 2009). The fracture network studied in this paper shows intensity variations within and between limestone layers. Potential controls on the intensity include bed thickness (e.g. Ladeira and Price, 1981; Narr and Suppe, 1991; Gross, 1993; Wu and Pollard, 1995; Ji and Saruwatari, 1998; Bai and

379 Pollard, 2000), lithology (e.g. Wennberg et al., 2006; Ortega et al., 2010; Afşar et al.,
380 2014) and structural position (e.g. Hanks et al., 1997; Watkins et al., 2015).

381 ### *Bed Thickness*

382 Statistical analysis of experiments 1, 2 and 3 suggests that there is little bed thickness
383 control on fracture intensity. P_{10} data from all four experiments show little correlation
384 with bed thickness (R = - 0.0015) (Section 4.5). This result is surprising as many
385 previous studies suggest that fracture intensity is inversely proportional to bed
386 thickness (Narr and Suppe, 1991; Wu and D. Pollard, 1995; Ji and Saruwatari, 1998).
387 Other studies (e.g. Ortega et al., 2010); Wennberg et al., 2006) suggest that bed
388 thickness does not influence fracture intensity and even that fracture intensities
389 actually increased with increasing bed thickness.(Ortega et al., 2010). Given the
390 stratabound nature of the joints and the clear indication of between-layer variation in
391 some of the experiments recorded here, if layer thickness is not a controlling factor
392 then what is?

393 ### *Lithology*

394 It is clear that lithology has a major effect on fracture intensity (Nelson 2001), as seen
395 in this study by the significant variation measured between the limestones and shales
396 (section 3.5). What is less obvious is whether lithological variations control the
397 intensity variation between the limestone beds. Thin sections show that the limestones
398 investigated in this study are homogenous and have little obvious variation in grain
399 size, clay content or texture.

400 Ortega et al. (2010) conclude that the level of dolomitization of the limestone is an
401 important factor controlling fracture intensity. Thin sections of the limestones show
402 no dolomite and, hence, it is not a controlling factor. Our limited investigation of the
403 petrography of the limestones does not allow us to eliminate all lithological controls

and there may be undiscovered factors, such as varying Young's modulus or Poisson's ratio between beds that contribute to the variation in stress and fracture intensity.

Rijken and Cooke (2001) suggest that an increase in the thickness of shale layers adjacent to limestone layers inhibits fracture propagation across the boundary layer interface and causes a higher percentage of stratabound fractures. The limestones in this study have surrounding marls and shales that are typically 2-5 times thicker than the limestones themselves. We found no significant variation in fracture intensity with the average thickness of adjacent shales.

Structural position

From the experiments, we conclude that there are significant spatial differences in the intensity of fracturing that will be discussed further in section 4.4. One possibility is that structural position could be controlling the variation in fractures. The two-way ANOVA of Experiments 3 and 4 suggest that there is a significant increase of fracture intensity in the footwall of an extensional fault, although this one example cannot be used to establish this as a general pattern. Rawnsley et al. (1998), however, state that the joints largely developed after the extensional faulting, and later than the subsequent inversion seen associated with some of them. It follows, therefore, that any control by faulting and associate wall-rock deformation (such as the buttress anticline discussed by Engelder and Peacock, 2001), must be indirect. Essentially we view the earlier fault-related deformation as creating a series of discontinuous blocks of layered strata. Subsequent loading of this complex architecture could then allow localization of stresses, producing local variation of the joint systems in proximity to earlier faults, as proposed by Rawnsley et al (1998). More subtly, the heterogeneous nature of the interlayered limestones and shales would produce strongly anisotropic materials, with varying orientations that are unlikely to respond homogeneously during uplift and joint development, even if the far field loading is reasonably uniform.

4.3 Evolution and development of fracture sets

Within the different layers, a total of five sets of joints are recognised, with different frequency and modal orientation, some sets being absent in some layers (Fig. 11a-d). For example, in Experiment 2, Set 2 is only developed in Bed 159 (Table 4, Fig. 11). Similar variation in the joint sets in different beds has also been noted by Engelder and Peacock (2001).

The joints developed after the extension and inversion of the basin, and are almost certainly due to the subsequent uplift and exhumation of the strata (Rawnsley et al., 1998; Peacock, 2001). The variety of joint trends means that some sets are sub-parallel to earlier faults, which has led to suggestions of a genetic link (e.g. Engelder and Peacock, 2001; Asfar et al., 2014). All fault phases have associated damage zones, containing fractures infilled with calcite. The later joints clearly cross-cut these and are not mineral filled (Peacock 2001). Rawnsley et al. (1998) describe joint sets that are perturbed around faults, which they attribute to local reactivation of faults. The entire sequence of joint development outlined in Fig. 11e is essentially post-inversion (i.e. late Miocene to Recent).

The analysis of abutting relationships at Y-nodes has revealed a sequence of sets designated 1 to 5 in order of development (Fig 11e). Although some joints are seen to cross-cut others, producing X-nodes, these are not abundant (usually 5% or less). Isolated nodes are also rare (again usually <5%), so the dominant nodes are Y-nodes (>90%). This produces a well-connected network, with a continual production of joints that are arrested at previously formed joints (Helgeson and Aydin, 1991). The earlier formed joints (Sets 1 and 2) extend for several meters, forming relatively straight systematic joints, except where perturbed by earlier faults, whereas the later formed joints are much shorter. Thus, the joint network can be interpreted as forming by a 'sequential infilling' (Bai and Pollard, 2000), with earlier joints appearing to act as mechanical layer boundaries to later joints that often curve to abut the earlier joints at

457 a high angle, forming cross-joints (e.g. Gross, 1993; Bai et al. 2002). As the joint sets
458 develop, the block size is progressively reduced and a range of block shapes
459 produced. Thus, the layering and earlier formed joints set up a complex and evolving
460 mechanical system that would be responsible for variation in fracture intensity. This
461 interpretation would explain the poor correlation between intensity and layer thickness
462 that is widely reported in many simple systems.

463 Since the maximum horizontal stress, σ_H, was approximately N-S during inversion and
464 the present-day stress has σ_H ~NW-SE (Baptie, 2010), it is not surprising that the
465 earlier formed joints (Sets 1 and 2) strike in a NW-SE direction. As uplift progressed
466 and more joints formed, the regional mean and differential stresses probably both
467 reduced, which would explain the greater variation in the orientation of the later joints.
468 Orientations appear to rotate anti-clockwise from set 1 to set 5, implying that the σ_H also
469 rotated anti-clockwise, as suggested by Rawnsley et al. (1998). An alternative
470 explanation is that the initial anti-clockwise rotation of σ_H from N-S to NW-SE would
471 have formed two sets of early joints. Fluctuation of σ_H about the NW-SE direction, in
472 response to local loading and varying block geometry, would have produced new
473 cross-joints if in an anti-clockwise direction, but could have simply reactivated existing
474 joints if in a clockwise direction.

475 ### *4.4 Mapping spatial variation*

476 The ANOVA indicates that there are at least two significant factors that control
477 fracturing within the limestone layers: (1) the variation between layers; and (2) the
478 variation with location (i.e. between experiments). The two-way ANOVA also indicates
479 that there can be significant interaction between these two factors. Hence it is
480 important to design future fracture surveys to recognise these sources of variability.
481 Possible strategies might include:

482 A. Sample only one particular limestone, thus eliminating between-limestone

variation; but this would lead to a very uneven distribution of data points.

B. Restrict the range of beds used with the aim of reducing between-layer effects; for example, by using similar limestones that are known to have similar intensities locally.

C. Design surveys with sufficient sample points to capture both the between-layer and regional spatial variation.

C is our favoured strategy, as it honours the observed variance. To illustrate strategy C, we chose the area of experiments 1 and 2 (Fig. 3) because these are close together and the area of experiment 1 had already been extended towards 2 in order to include exposures of bed 165. We added 6 new sample sites between the two experiments to provide a better coverage. The P_{10} data and a hand contoured map are shown in Fig 12a. Note that the contours apply only to the intensity in the limestone layers, and do not represent values in the intervening shales. The data and contours have been projected onto an E-W trending cross-section in Fig. 12b.

In beds 155, 159 and 165, P_{10} decreases from E to W, reflecting a regional trend in the fracture intensity, but there is little overall change in beds 157 and 161. In the east (Experiment 1) there is much less variation between beds than in the west (Experiment 2). An alternative view of this variation is that high fracture intensity in the east is channelled along beds 161 and 157, suggesting a fundamental difference in the spatial variation from bed to bed (Fig. 12b).

The map (Fig. 12a), and particularly the section (Fig. 12b), indicate the interaction between the layers and a general increase in intensity from west to east. Combining this with the observation that the joint sets vary from layer to layer (Fig. 11), suggests that the distribution of joints is controlled by both structural position and layering.

Strategy A would lead to a very uneven distribution of data points, with large gaps appearing where the selected bed was not exposed. It also follows from the large

between-layer variations, that somewhat different maps and trends would be produced depending on the bed chosen.

The between-layer variation seen in this study would make selection of layers difficult in strategy B. Using all 5 layers targeted in this study and ignoring their position when contouring the intensity, would produce a rather 'noisy' map, with many 'bull's eyes' around individual samples and 'interdigitation' of high and low intensities, as is seen in Fig. 12a, but without the reference of the layering to guide interpretation.

The main drawback to strategy C is that it requires very dense sampling to capture the influence of layering. Using Fig. 12a as a guide, would suggest that ~500 sample sites per km^2 would be needed in an area such as the one studied in this paper. This emphasises the need for efficient sampling techniques, as discussed in section 4.1, but may be limited by the availability of suitable exposed surfaces.

5. Conclusions

The topological sampling used in this study combines two ideas: 1) node counting and 2) using a circular sampling area. The methods allow fracture intensity to be measured to similar levels of precision as more traditional methods, with the resulting fracture intensity (P_{10}) being in good agreement with that obtained from 2-D trace mapping (P_{21}). The method allows ~10 times faster collection of data; thus it greatly improves the efficiency of fracture studies, providing a new approach to the design of fracture surveys.

In addition to rapid measurement of intensity, counting different node types within a sample area allows evaluation of the topology of the fracture network. By combining intensity estimates with these node types, one can also estimate additional parameters such as average trace length and branch length. These in turn allow estimates of dimensionless intensity, which are useful in the assessment of connectivity (Sanderson and Nixon 2015).

If the sample circles are photographed and digitally restored, the resulting images may be georeferenced in a GIS and further analysed. This allows measurement of trace lengths and orientations, providing independent estimates of intensity (P_{21}). The GIS results can be used to identify joint sets and analyse the sequence of fracturing, with the joint development being shown to vary somewhat from bed to bed.

A series of 'experiments' were designed to assess the between-layer variability of joints in an interbedded limestone/shale sequence. A significant difference in fracture intensity occurs between the limestone and shale. ANOVA methods also show that there is a significant difference in fracture intensity between the limestone beds in two of the four experiments. This variation is not simply due to bed thickness, nor is it related to any obvious compositional or textural variation between the limestone beds. Two-way ANOVA also indicates that there is variability in fracture intensity both between layers and regionally (between experiments).

From these results we discuss approaches to the spatial mapping of fracture intensity. A small pilot study, of data collected in a few days, suggests that sampling of ~500 sites per square km may be necessary in limestone/shale sequences interbedded on the ~1 m scale. Thus there is a need to carefully assess the sources of variation in fracture intensity and to design sampling strategies for fracture surveys accordingly.

6. Acknowledgements

This work forms part of a MSci project by Andres Procter in Ocean and Earth Sciences at the University of Southampton. We thank Casey Nixon for help with ArcGIS and extraction of nodes and branches. We would also like to thank the reviewers (John Hooker and unknown) and editors (Steve Laubach, and Bill Dunne) for their helpful and insightful comments that helped improve the manuscript.

7. References

Afşar, F., Westphal, H., Philipp S.L. 2014. How facies and diagenesis affect fracturing of limestone beds and reservoir permeability in limestone–marl alternations. Marine and Petroleum Geology 57, 418-432.

Antonellini, M., Aydin, A. 1994. Effect of faulting on fluid flow in porous sandstones: petrophysical properties. AAPG Bulletin 78, 355–377.

Bai, T., Maerten, L., Gross, M.R., Aydin, A. 2002. Orthogonal cross joints: do they imply a regional stress rotation? Journal of Structural Geology 24, 77-88.

Bai, T., Pollard, D.D. 2000. Fracture spacing in layered rocks: a new explanation based on the stress transition. Journal of Structural Geology 22, 43-57.

Baptie, B. 2010. Seismogenesis and state of stress in the UK. Tectonophysics 482, 150-159.

Chadwick, R. 1986. Extension tectonics in the Wessex Basin, southern England. Journal of the Geological Society 143, 465-488.

Dart, C.J., McClay, K., Hollings, P.N. 1995. 3D analysis of inverted extensional fault systems, southern Bristol Channel basin, UK. In: Buchanan, J.G., Buchanan, P.G. (eds), Basin Inversion, Geological Society London Special Publications 88, 393-413.

Dershowitz, W.S., Herda, H.H. 1992. Interpretation of fracture spacing and intensity. In 33rd US Symposium on Rock Mechanics, Santa Fe, NM, pp. 757-766.

Einstein, H.H., Baecher, G.B. 1983. Probabilistic and statistical methods in engineering geology. Rock Mechanics and Rock Engineering 16, 39-72.

Engelder, T., Peacock, D.C.P. 2001. Joint development normal to regional compression during flexural-flow folding: the Lilstock buttress anticline, Somerset, England. Journal of Structural Geology 23, 259-277.

586 Gross, M.R. 1993. The origin and spacing of cross joints: examples from the Monterey
587 Formation, Santa Barbara Coastline, California. Journal of Structural Geology
588 15, 737-751.
589 Hancock, P.L. 1985. Brittle microtectonics: principles and practice. Journal of
590 Structural Geology 7, 437-457.
591 Hanks, C.L., Lorenz, J., Teufel, L., Krumhardt, A.P. 1997. Lithologic and structural
592 controls on natural fracture distribution and behavior within the Lisburne Group,
593 northeastern Brooks Range and North Slope subsurface, Alaska. AAPG
594 Bulletin 81, 1700-1720.
595 Helgeson, D.E., Aydin, A. 1991. Characteristics of joint propagation across layer
596 interfaces in sedimentary rocks. Journal of Structural Geology 13, 897-911.
597 Hooker, J.N., Laubach, S.E., Marrett, R., 2013. Fracture-aperture sized frequency,
598 spatial distribution, and growth processes in strata-bounded and non-
599 stratabounded fractures, Cambrian Meson Group, NW Argentina. Journal of
600 Structural Geology 54, 54-71.
601 Ji, S., Saruwatari, K. 1998. A revised model for the relationship between joint spacing
602 and layer thickness. Journal of Structural Geology 20, 1495-1508.
603 Ladeira, F.L., Price, N.J. 1981. Relationship between fracture spacing and bed
604 thickness. Journal of Structural Geology 3, 179-183.
605 Larsen, B., Gudmundsson, A. 2010. Linking of fractures in layered rocks: Implications
606 for permeability. Tectonophysics 492, 108-120.
607 Long, J.C.S., Witherspoon, P.A. 1985. The relationship of the degree of
608 interconnection to permeability in fracture networks. Journal of Geophysical
609 Research 90, 3087.
610 Macias, F.J., Jakobsen, P.D., Seo, Y. Bruland, A. 2014. Influence of rock mass
611 fracturing on the net penetration rates of hard rock TBMs. Tunnelling and
612 Underground Space Technology 44, 108-120.

613 Manzocchi, T., 2002. The connectivity of two dimensional networks of spatially
614 correlated fractures. Water Resources Research 38,10.1029/2000WR000180.
615 Marrett, R.A., Ortega, O.J., Kelsey, C. 1999. Extent of power-law scaling for natural
616 fractures in rock. Geology 27, 799– 802.
617 Mauldon, M., Dunn, W.M., Rohrbaugh, M.B. 2001. Circular scanlines and circular
618 windows: new tools for characterizing the geometry of fracture traces. Journal
619 of Structural Geology 23, 247-258.
620 Narr, W., Suppe, J. 1991. Joint spacing in sedimentary rocks. Journal of Structural
621 Geology 13, 1037-1048.
622 Nelson, R.A. 2001. Geologic Analysis of Naturally Fractured Reservoirs (Second
623 edition). Woburn, Gulf Professional Publishing, 125-162.
624 Odling, N.E. 1997. Scaling and connectivity of joint systems in sandstones from
625 western Norway, Journal of Structural Geology 19, 1257–1271.
626 Olson, J.E., Laubach, S.E., Lander, R.H., 2009. Natural fracture characterization in
627 tight gas sandstones: integrating mechanics and diagenesis. AAPG Bulletin 93,
628 1535-1549.
629 Ortega, O.J., Gale, J.F.W., Marret, R.A. 2010. Quantifying diagenetic and stratigraphic
630 controls on fracture intensity in platform carbonates: An example from the
631 Sierra Madre Oriental, northeast Mexico. Journal of Structural Geology 32,
632 1943-1959.
633 Ortega, O.J., Marrett, R.A., Laubach, S.E. 2006. A scale-independent approach to
634 fracture intensity and average spacing measurement. AAPG Bulle 90, 193-208.
635 Palmstrøm, A. 1996. Characterizing rock masses by the RMi for use in practical rock
636 engineering: Part 1: The development of the Rock Mass index (RMi).
637 Tunnelling and Underground Space Technology 11, 175-188.
638 Peacock, D.C.P. 2001. The temporal relationship between joints and faults. Journal of
639 Structural Geology 23, 329-341.

640 Peacock, D.C.P., Sanderson, D.J. 1999. Deformation history and basin-controlling
641 faults in the Mesozoic sedimentary rocks of the Somerset coast. Proceedings
642 of the Geologists' Association 110, 41-52.
643 Priest, S.D., 1993. Discontinuity Analysis for Rock Engineering. Chapman & Hall, New
644 York, 473 pp.
645 Priest, S.D., Hudson, J.A., 1981. Estimation of discontinuity spacing and trace length
646 using scanline surveys. International Journal of Rock Mechanics & Mining
647 Sciences 18, 183-197.
648 Quesada, D., Picard, D., Putot, C., Leguillon, D. 2009. The role of the interbed
649 thickness on the step-over fracture under overburden pressure. International
650 Journal of Rock Mechanics and Mining Sciences 46, 281- 288.
651 Rawnsley, K.D., Peacock, D.C.P., Rives, T., Petit, J.-P. 1998. Joints in the Mesozoic
652 sediments around the Bristol Channel Basin. Journal of Structural Geology 20,
653 1641-1661.
654 Rijken, P., Cooke, M.L. 2001. Role of shale thickness on vertical connectivity of
655 fractures: application of crack-bridging theory to the Austin Chalk, Texas.
656 Tectonophysics 337, 117-133.
657 Rohrbaugh, M.B., Dunne, W.M., Mauldon, M. 2002. Estimating fracture trace intensity,
658 density, and mean length using circular scan lines and windows. AAPG Bulletin
659 86, 2089-2104.
660 Sanderson, D.J., Nixon, C.W. 2015. The use of topology in fracture network
661 characterization. Journal of Structural Geology 72, 55-66.
662 Sanderson, D.J. 2015. Field-based structural studies as analogues to sub-surface
663 reservoirs. In: Bowman, M., Smyth, H.R., Good, T.R., Passey, S.R., Hirst,
664 J.P.P. & Jordan, C.J. (eds) The Value of Outcrop Studies in Reducing
665 Subsurface Uncertainty and Risk in Hydrocarbon Exploration and Production.
666 Geological Society London, Special Publications, 436,
667 http://doi.org/10.1144/SP436.5

668 Sheppard, T.H., Houghton, R.D. Swan, A.R.H. 2006. Bedding and pseudo-bedding in
669 the Early Jurassic of Glamorgan: deposition and diagenesis of the Blue Lias in
670 South Wales. Proceedings of the Geologists' Association 117 249-264.
671 Singhal, B.B.S., Gupta, R.P. 2010. Fractures and Discontinuities. In: Singhal, B.B.S.,
672 Gupta, R.P. (eds) Applied Hydrogeology of Fractured Rock. Springer, 13-33.
673 Terzaghi, R.D. 1965. Sources of error in joint surveys. Geotechnique 15, 287-304.
674 Van Hoorn, B. 1987. The south Celtic Sea/Bristol Channel Basin: origin, deformation
675 and inversion history. Tectonophysics 137, 309-334.
676 Villaescusa, E., Brown, E. 1992. Maximum likelihood estimation of joint size from trace
677 length measurements. Rock Mechanics and Rock Engineering 25, 67-87.
678 Watkins H., Bond C.E., Healy D., Butler, R.W.H. 2015. Appraisal of fracture sampling
679 methods and a new workflow to characterise heterogeneous fracture networks
680 at outcrop. Journal of Structural Geology 72, 67-82.
681 Watkins, H., Butler, R.W.H., Bond C.E., Healy D. 2015. Influence of structural position
682 on fracture networks in the Torridon Group, Achnashellach fold and thrust belt,
683 NW Scotland. Journal of Structural Geology 74, 64-80.
684 Wennberg, O., Svånå, T., Azizzadeh, M., Aqrawi, A.M.M., Brockbank, P., Lyslo, K.B.,
685 Ogilvie, S. 2006. Fracture intensity vs. mechanical stratigraphy in platform top
686 carbonates: the Aquitanian of the Asmari Formation, Khaviz Anticline, Zagros,
687 SW Iran. Petroleum Geoscience 12, 235-246.
688 Whittaker, A., Green, G.W. 1983. Geology of the country around Weston-super-Mare,
689 HM Stationery Office.
690 Wu, H., Pollard, D.D. 1995. An experimental study of the relationship between joint
691 spacing and layer thickness. Journal of Structural Geology 17, 887-905.
692 Zimmerman R, Main I, 2003. Hydromechanical behavior of fractured rocks. In:
693 Gueguen Y, Bouteca M. (eds) Mechanics of Fluid Saturated Rocks.
694 International Geophysics Series 89, 361-419.

8. Figure Captions

Fig. 1 Map showing location of area studied in North Somerset, UK.

Fig. 2 Photograph (a) and simplified log (b) of beds examined in this study. Bed numbers based on Whittaker and Green (1983).

Fig. 3 Aerial photograph of section between East Quantoxhead and Kilve, showing locations of experiments.

Fig.4 (a) Node and branch system used to describe networks; Lines represent fracture traces, with one fracture A-B highlighted; circle – I-node, triangle – Y-node; square – X-node (after Sanderson and Nixon 2015). (b) Circle sampling of node types, stars are edge nodes where fracture traces intersect circle; (c) Triangular plot of proportions of nodes used in topological characterization.

Fig.5 Diagram showing proposed workflow for fracture characterization; large boxes indicate division into field and laboratory based procedures.

Fig.6 (a) Field photograph of site Q9-155 from Experiment 1, demonstrating the process of node counting in the field. Red counters are placed on edge nodes on the circular scanline and on I- and X-nodes; green counters on Y-nodes. The number of each type of node is counted and recorded. The compass points north (arrow). (b) Rectified photograph; (c) digitized nodes and branches; (d) interpretation of fracture sets, with set numbers used in Table 4.

Fig.7 Plot of 2-dimensional intensity (P_{21}) from GIS against 1-dimensional intensity (P_{10}) from counting edge nodes for four beds in Experiment 2.

Fig.8 Box-and-whisker plot of intensity (P_{10}) in the four experiments: 'box' - 95% confidence limits around mean, 'whisker' - range. For experiments 2 and 4 the high and low intensity beds are indicated solid red and dashed blue lines respectively.

720 Fig. 9 (a) Plot of intensity (P_{10}) against bed thickness for all experiments. (b) Box-
721 and-whisker plot of intensity (P_{10}) as in Fig. 8.

722 Fig. 10 IYX triangular plot showing Y-dominated, highly-connected nature of the
723 fracture network in limestone beds, and the poorly-connected, IY topology in the
724 shales.

725 Fig. 11 Rose diagrams of joint orientations in beds (a) 155, (b) 157, (c) 159 and (d)
726 161 in experiment 2, with set numbers identified. (e) Sequence of set development
727 deduced from abutting relationships at Y-nodes, numbers of observations indicated;
728 solid lines indicate main sequence; dashed lines indicate some "backcycling", as
729 discussed in text.

730 Fig. 12 (a) Contour map of area of Experiments 1 and 2, with some infill sites,
731 showing fracture intensity in three intervals: <3.5 m-1, 3.5-5 m-1, >5 m-1. (b) Same
732 data projected onto E-W oriented cross-section. Colours indicate low (light blue) to
733 high (red) fracture intensities.

9. Tables

Table 1 Summary of beds used in each experiment, with number of samples (n) and mean intensity <P_{10}>; X indicated beds used in ANOVA tests.

Experiment	155	157	159	161	165	all	Thin	Shale
1	X	X	X	X	X			
n	3	3	3	3	3	15	3	6
<P_{10}>	3.83	4.67	6.17	5.58	2.63	5.18	6.0	0.51
2	X	X	X	X	X			
n	4	6	5	3	4	22		
<P_{10}>	2.88	5.13	3.50	6.25	2.63	4.05		
3		X	X	X				
n		6	2	3		11		
<P_{10}>		5.48	3.88	4.92		5.03		
4		X	X	X				
n		2	3	3		8		
<P_{10}>		3.44	3.29	4.54		3.80		

Table 2 Results from Analysis of Variance (ANOVA) in the four experiments. DF – degrees of freedom; SSDev – Sum of squared deviations; MSD – mean squared devistion; F- F-ratio; P – probability.

	DF	*SSDev*	*MSD*	*F*	*P*	
Experiment 1						
between	4	10.35	2.59	2.17	0.146188	NS
within	10	11.93	1.19			
total	14	22.28				
Experiment 2						
between	4	36.61	9.15	21.55	0.000002	***
within	17	7.22	0.42			
total	21	43.83				
Experiment 3						
between	2	3.92	1.96	3.49	0.081440	NS
within	8	4.49	0.56			
total	10	8.41				
Experiment 4						
between	2	2.69	1.34	13.51	0.0096	**
within	5	0.50	0.10			
total	7	3.19				

742 Table 3a: Two-way ANOVA based on triplicate samples from beds 155, 157, 159, 161
743 and 165 in Experiments 1 and 2; nomenclature as Table 2.

Source of Variation	*SS*	*df*	*MS*	*F*	*P-value*	
Experiments	9.35	1	9.35	11.24	0.0032	**
Layers	23.90	4	5.98	7.18	0.00093	***
Interaction	18.51	4	4.63	5.56	0.0035	**
Within	16.64	20	0.83			
Total	68.40	29				

744

745 Table 3b: Two-way ANOVA based on duplicate samples from beds 157, 159, and
746 161 in Experiments 3 and 4; nomenclature as Table 2.

Source of Variation	*SS*	*df*	*MS*	*F*	*P-value*	
Experiments	5.67	1	5.67	13.28	0.011	*
Layers	4.82	2	2.41	5.65	0.042	*
Interaction	2.84	2	1.42	3.33	0.106	NS
Within	2.56	6	0.43			
Total	15.90	11				

747

748

749 Table 4: Fracture sets identified in Experiment 2, with presence in each bed

Set	Orientation	Description	155	157	159	161
1	160° ± 20°	Long (>5 m), NW-SE striking fractures that generally run through the sampling circles	X	X		X
2	130° ± 25°				X	
3	095° ± 30°	E-W striking fractures that generally abut Sets 1 and 2.	X	X		X
4	040° ± 40°	Short (<1 m), curved fractures with variable trend that generally abut Sets 1 – 3.	X	X	X	
5	010° ± 40°		X		X	X

750

Figure 1

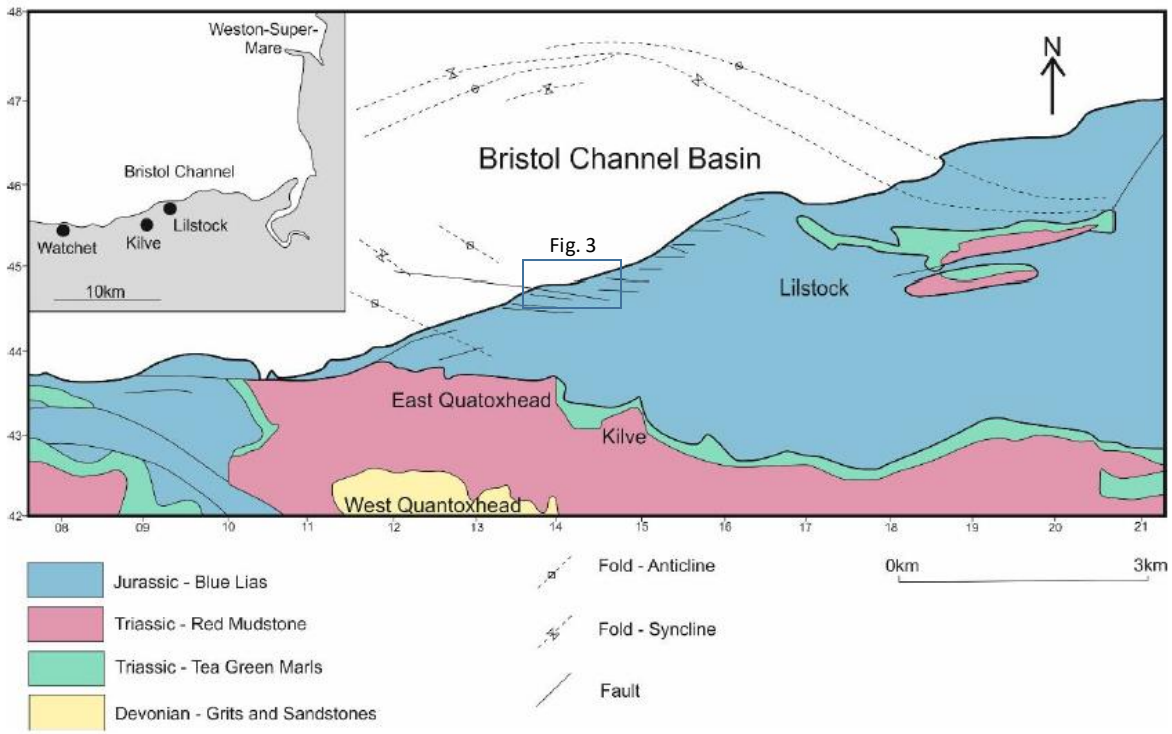
Weston-Super-Mare
Bristol Channel
Watchet
Kilve
Lilstock
10km
Bristol Channel Basin
Fig. 3
Lilstock
East Quatoxhead
Kilve
West Quantoxhead
N
48
47
46
45
44
43
42
08
09
10
11
12
13
14
15
16
17
18
19
20
21
Jurassic - Blue Lias
Triassic - Red Mudstone
Triassic - Tea Green Marls
Devonian - Grits and Sandstones
Fold - Anticline
Fold - Syncline
Fault
0km
3km

Figure 2

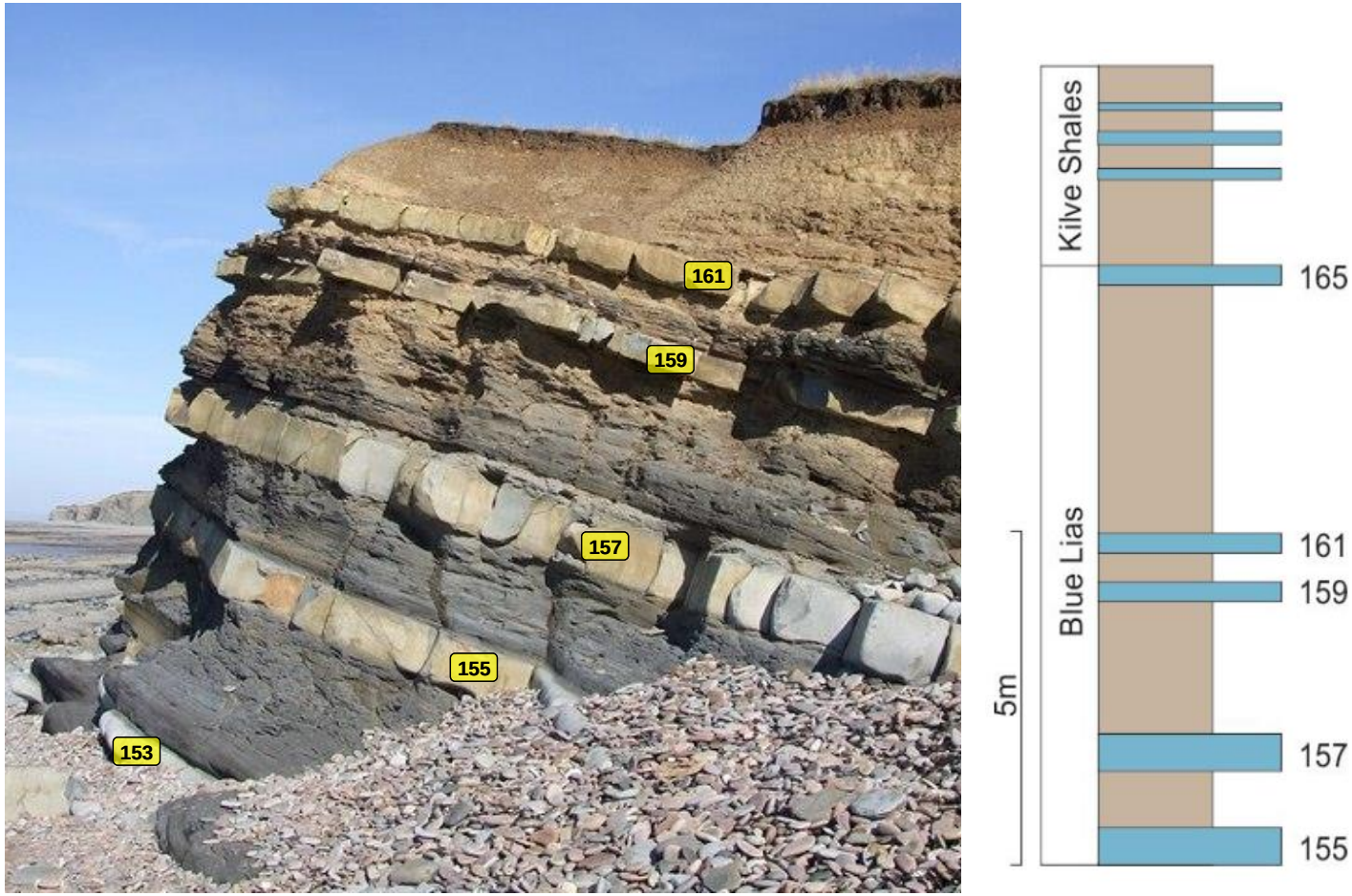
161
159
157
155
153
Kilve Shales
Blue Lias
5m
165
161
159
157
155

Figure 3

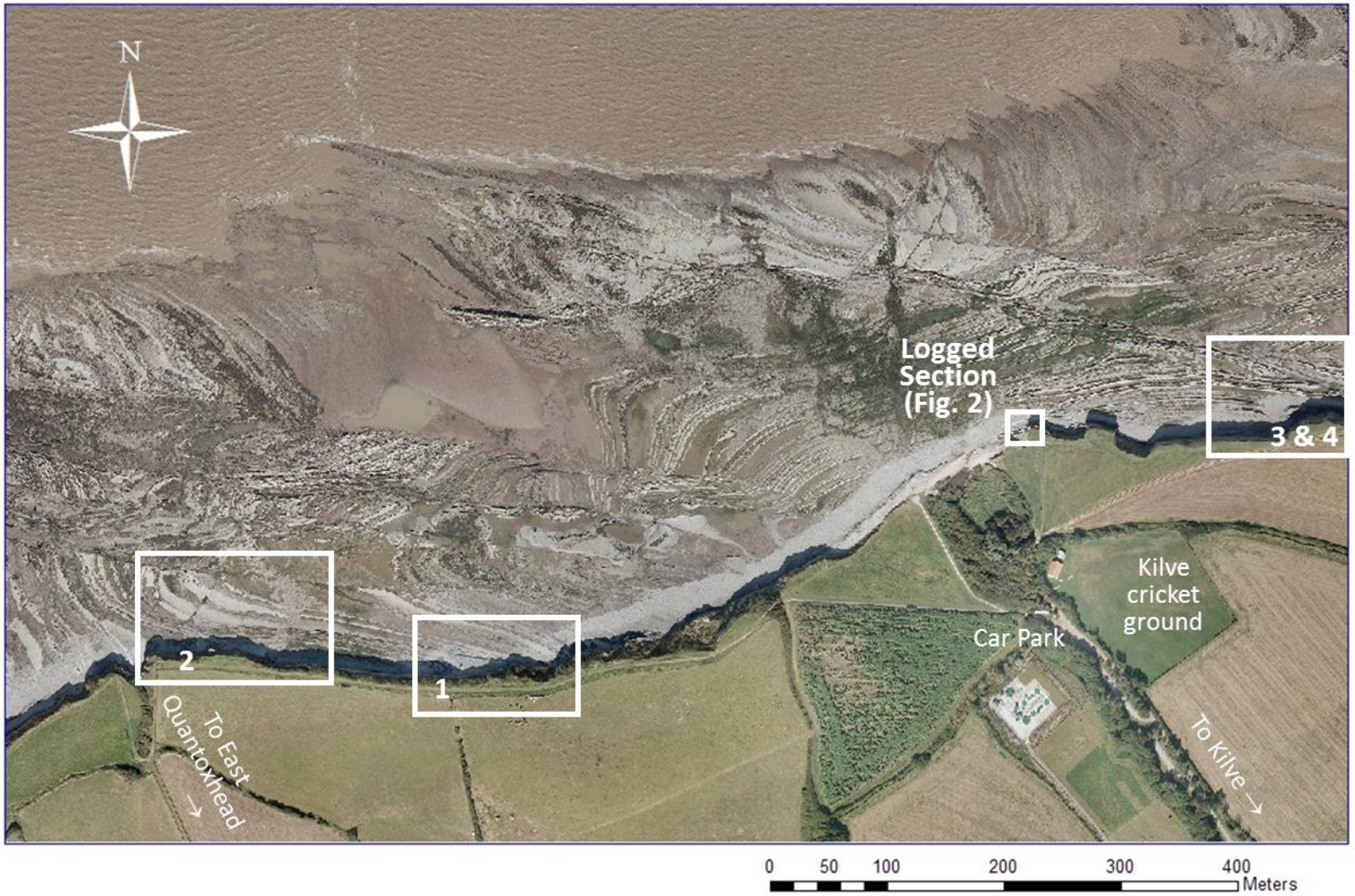
N
Logged Section (Fig. 2)
3 & 4
2
1
Kilve cricket ground
Car Park
To East Quantoxhead →
To Kilve →
0 50 100 200 300 400
Meters

Figure 4

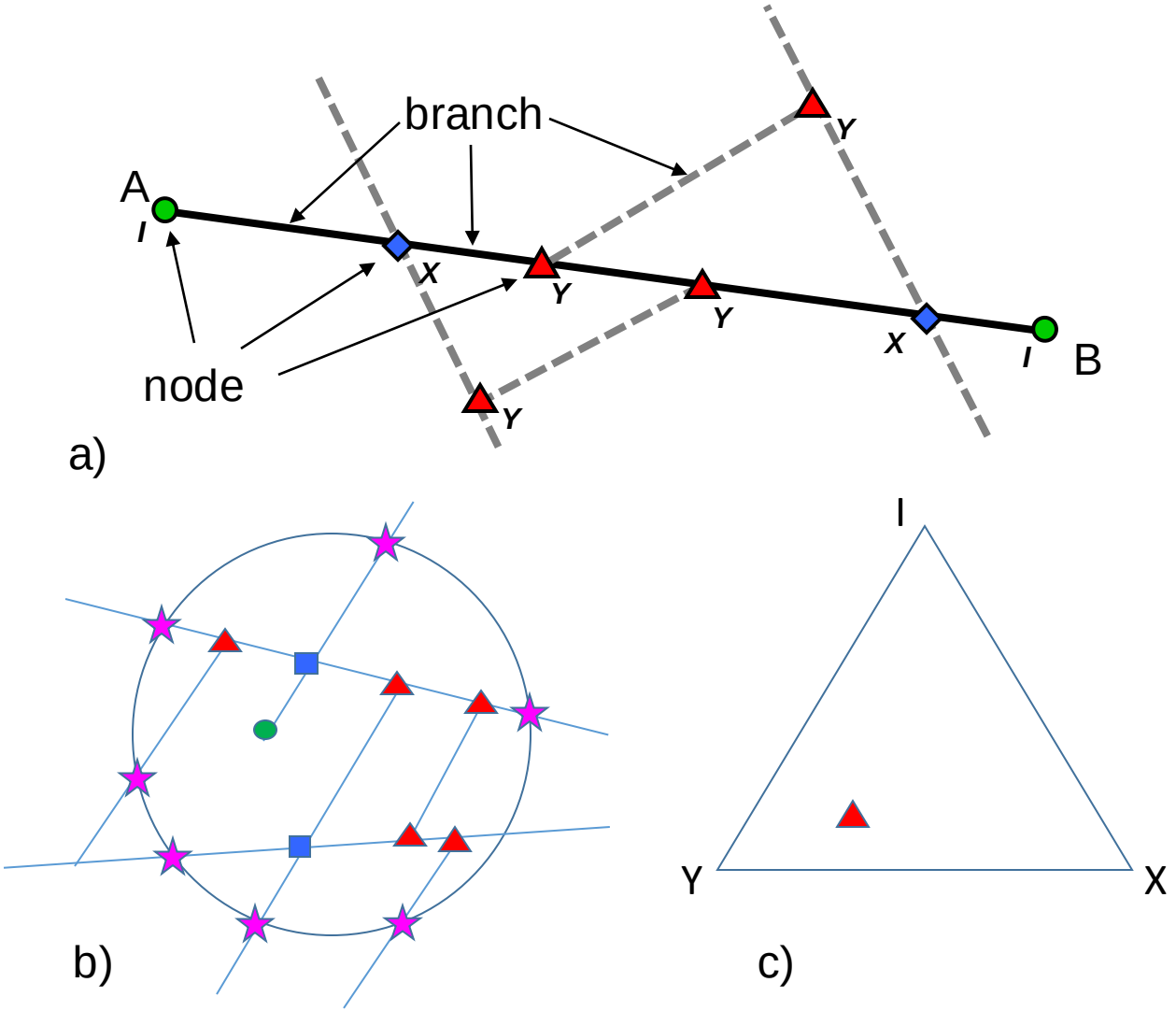

Figure 5

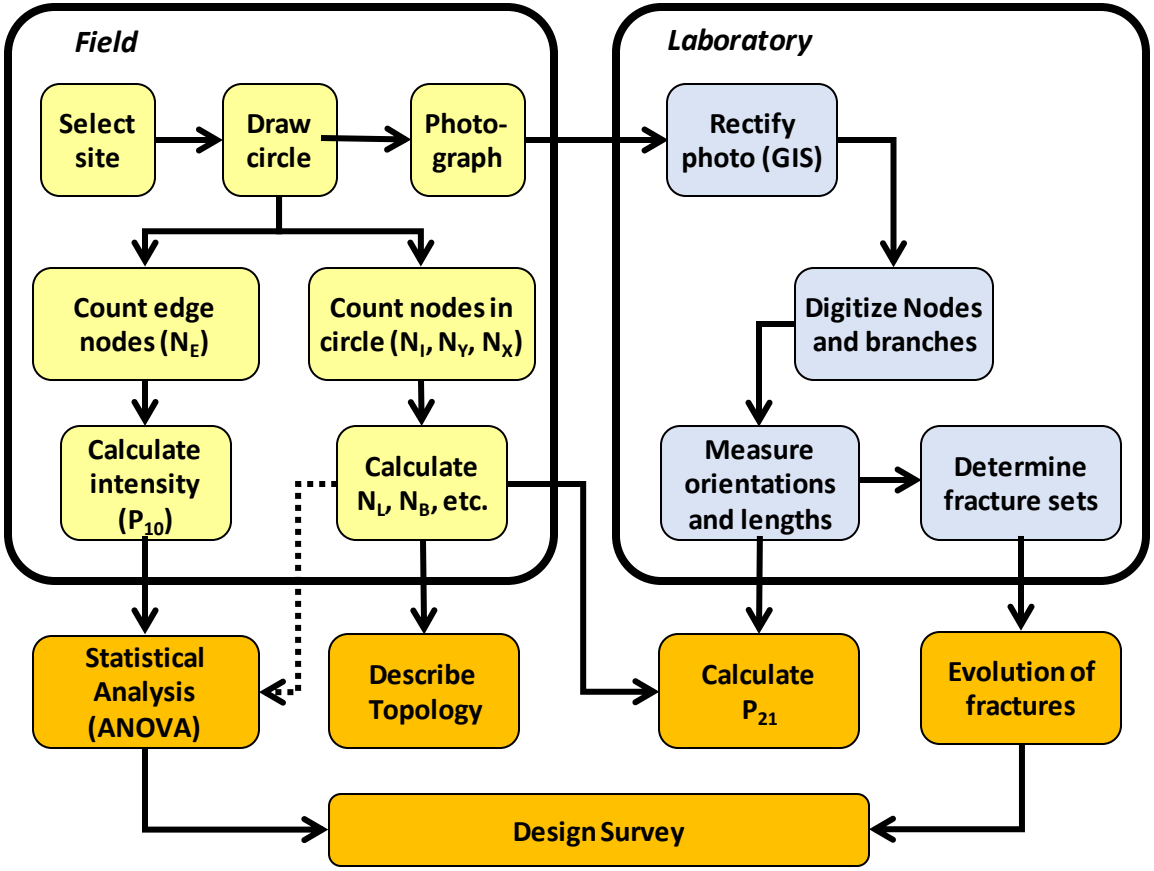
Field
Laboratory
Select site
Draw circle
Photo-graph
Rectify photo (GIS)
Count edge nodes (N_E)
Count nodes in circle (N_I, N_Y, N_X)
Digitize Nodes and branches
Calculate intensity (P_{10})
Calculate N_L, N_B, etc.
Measure orientations and lengths
Determine fracture sets
Statistical Analysis (ANOVA)
Describe Topology
Calculate P_{21}
Evolution of fractures
Design Survey

Figure 6

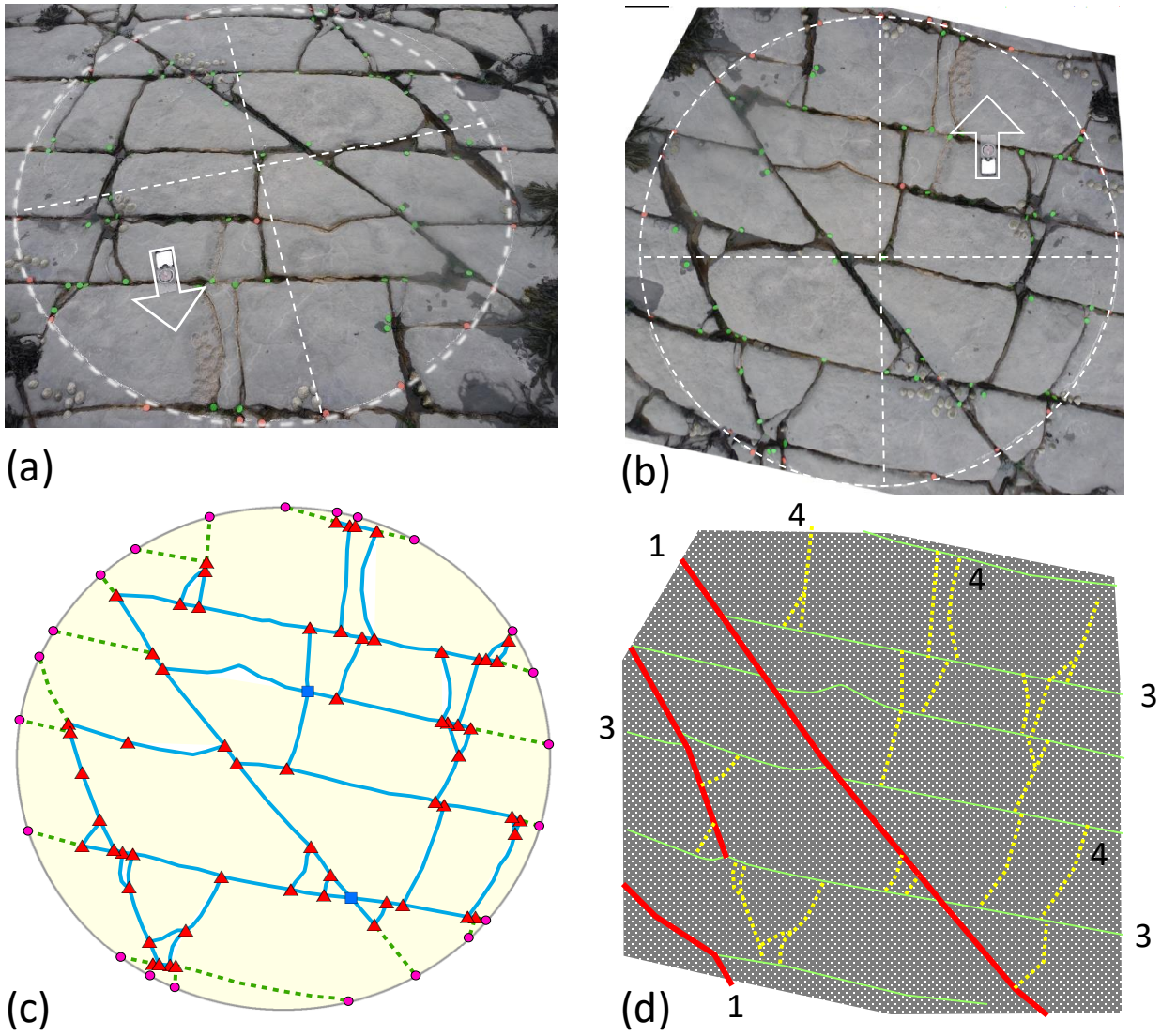

Figure 7

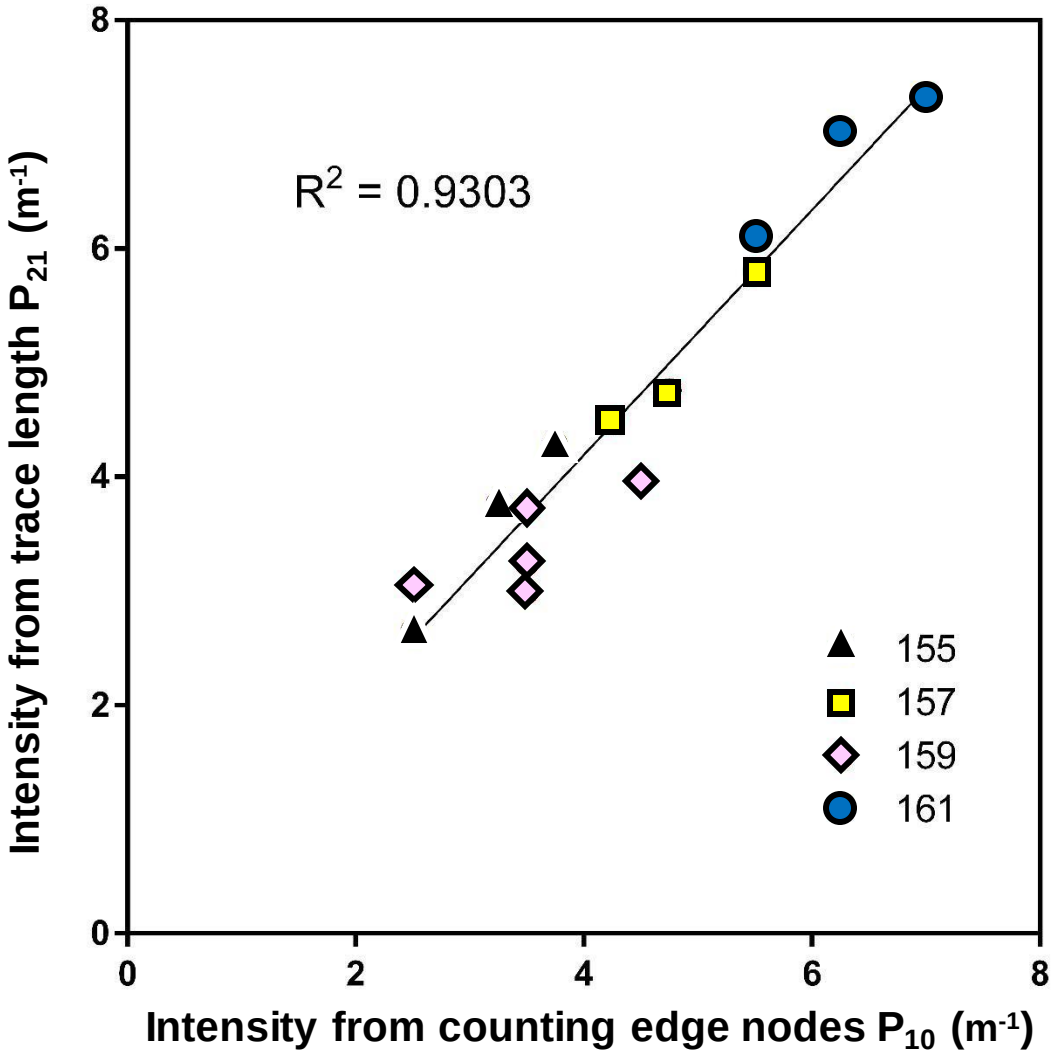
R^2 = 0.9303
Intensity from trace length P_{21} (m^{-1})
Intensity from counting edge nodes P_{10} (m^{-1})
0
2
4
6
8
155
157
159
161

Figure 8

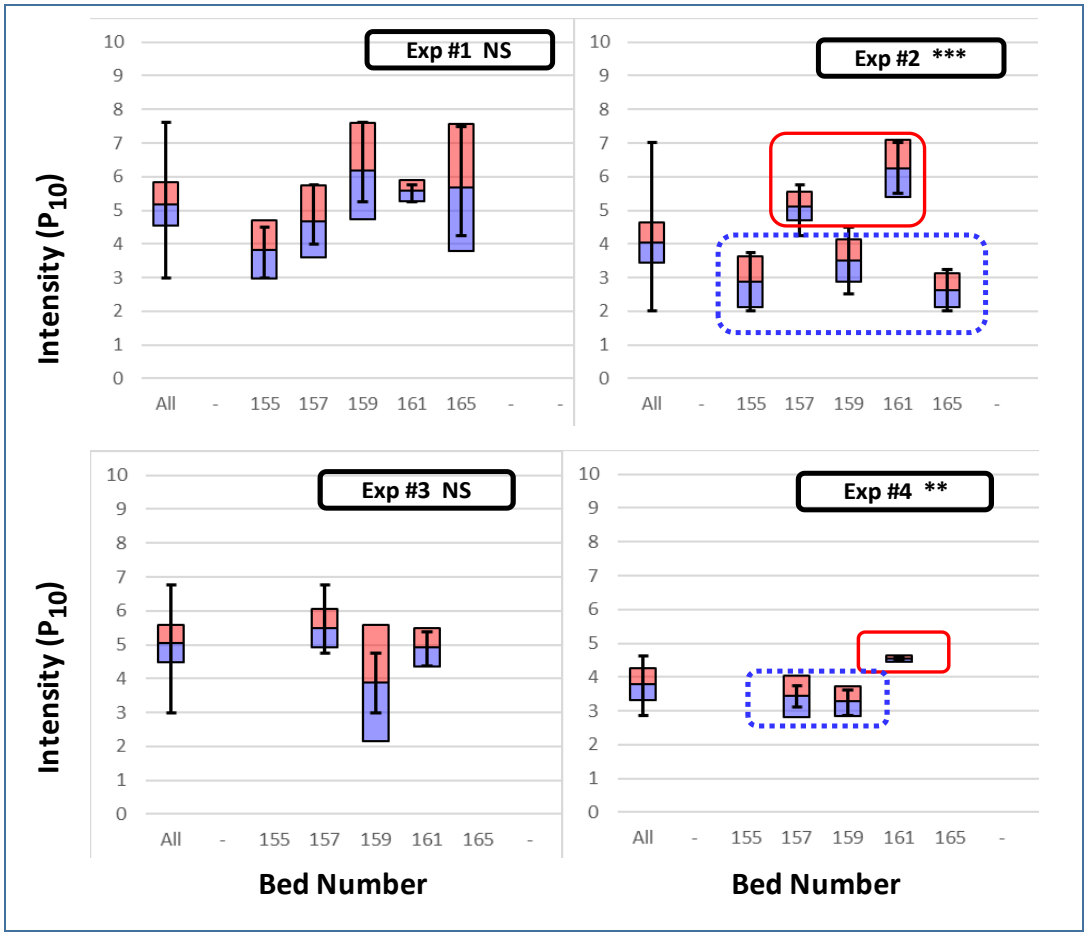
Exp #1 NS
Exp #2 ***
Exp #3 NS
Exp #4 **
Intensity (P10)
Intensity (P10)
10
9
8
7
6
5
4
3
2
1
0
All
-
155
157
159
161
165
-
-
Bed Number
Bed Number

Figure 9

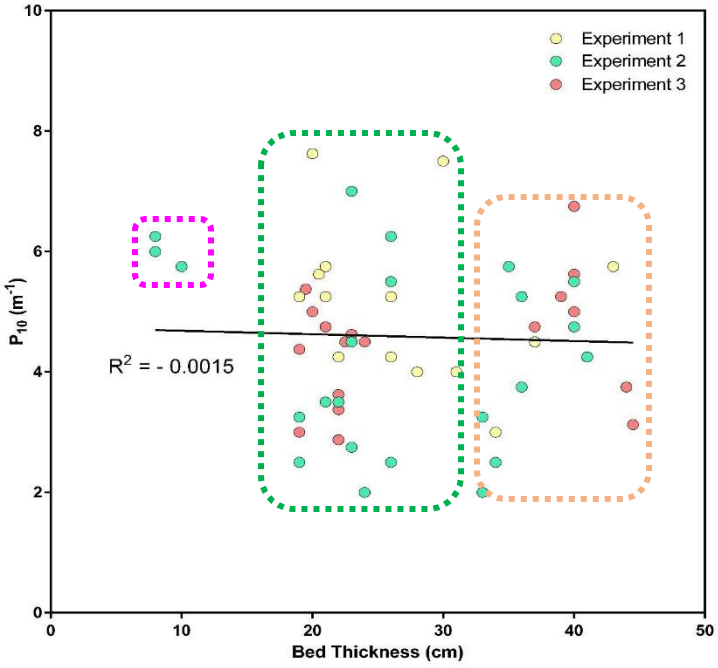
Experiment 1
Experiment 2
Experiment 3
R^2 = - 0.0015
P_{10} (m^{-1})
Bed Thickness (cm)
0
2
4
6
8
10
0
10
20
30
40
50

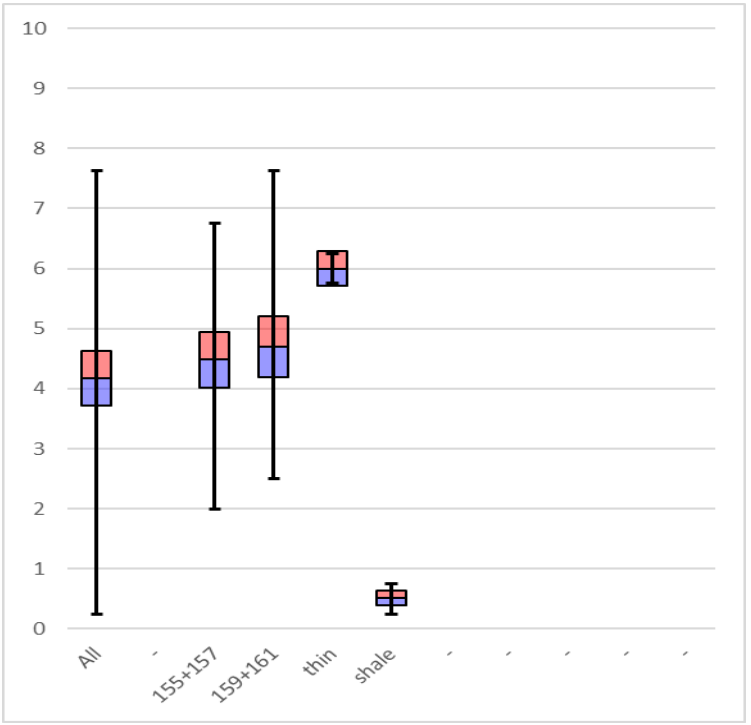
0
1
2
3
4
5
6
7
8
9
10
All
155+157
159+161
thin
shale

Figure 10

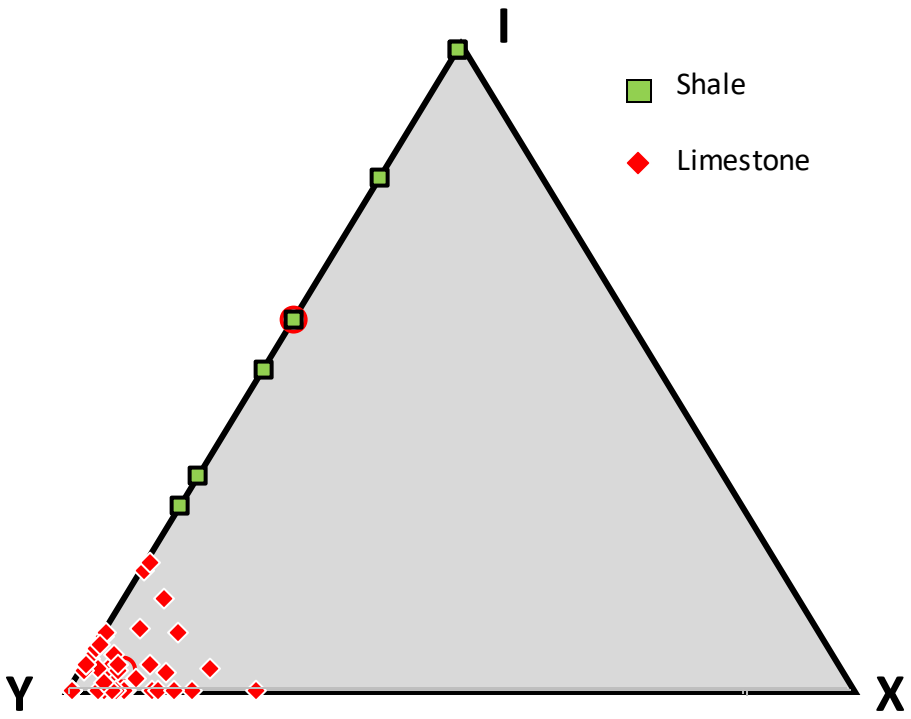

Figure 11

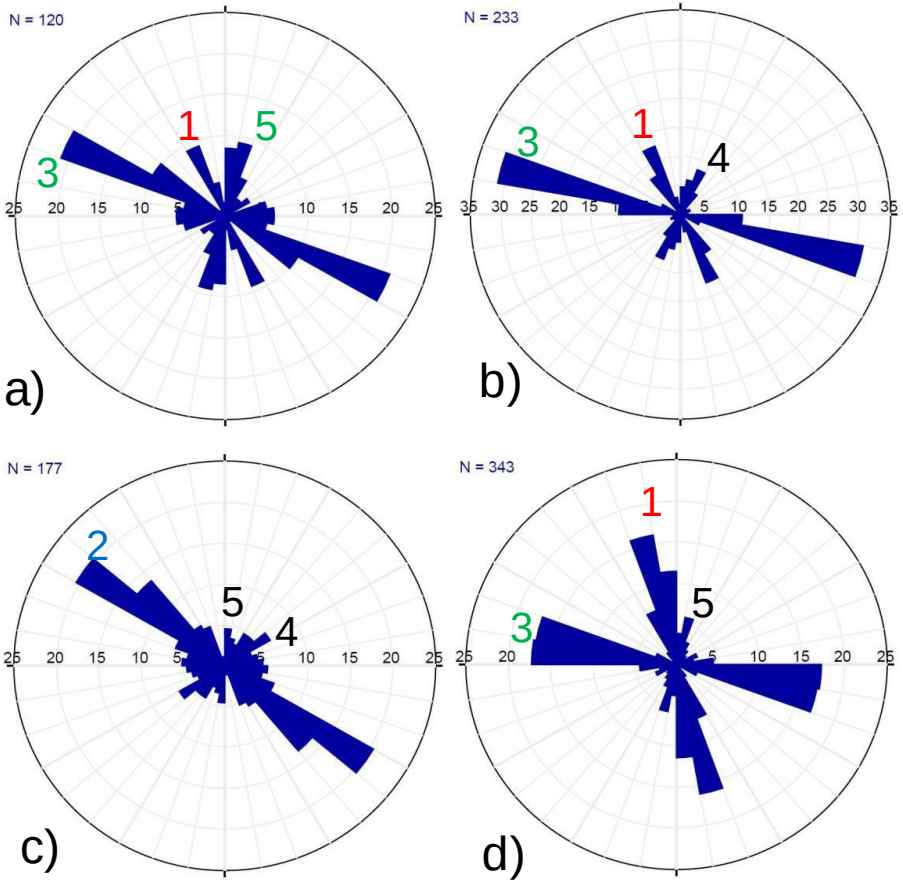
N = 120
1
5
3
a)
N = 233
3
1
4
b)
N = 177
2
5
4
c)
N = 343
1
5
3
d)

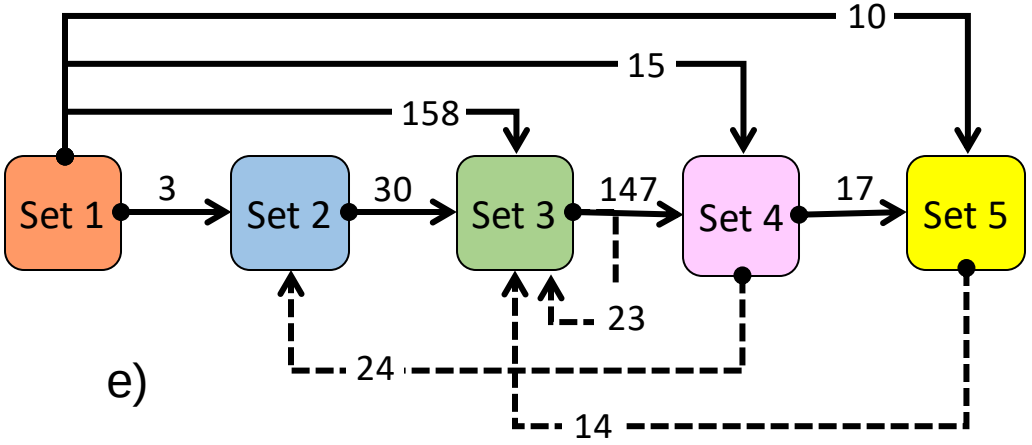
10
15
158
Set 1
3
Set 2
30
Set 3
147
Set 4
17
Set 5
23
24
14
e)

Figure 12